Morphological and functional abnormalities in mitochondria associated with synaptic degeneration in prion disease

The American Journal of Pathology, Vol. 177, No. 3, September 2010

DOI: 10.2353/ajpath.2010.091037

Neurobiology

Morphological and Functional Abnormalities in Mitochondria Associated with Synaptic Degeneration in Prion Disease

Zuzana Sisková,* Don Joseph Mahad,† Carianne Pudney,* Graham Campbell,† Mark Cadogan,† Ayodeji Asuni, Vincent O'Connor,* and Victor Hugh Perry

From the CNS Inflammation Group, School of Biological Sciences, University of Southampton, Southampton, United Kingdom; and The Mitochondrial Research Group,† Newcastle University, Newcastle, United Kingdom.*

Synaptic and dendritic pathology is a well-documented component of prion disease. In common with other neurodegenerative diseases that contain an element of protein misfolding, little is known about the underlying mechanisms of synaptic degeneration. In particular, in prion disease the relationship between synaptic malfunction, degeneration, and mitochondria has been neglected. We investigated a wide range of mitochondrial parameters, including changes in mitochondrial density, inner membrane ultrastructure, functional properties and nature of mitochondrial DNA from hippocampal tissue of mice with prion disease, which have ongoing synaptic pathology. Our results indicate that despite a lack of detectable changes in either mitochondrial density or expression of the mitochondrial proteins, mitochondrial function was impaired when compared with age-matched control animals. We observed changes in mitochondrial inner membrane morphology and a reduction in the cytochrome c oxidase activity relative to a sustained level of mitochondrial proteins such as porin and individual, functionally important subunits of complex II and complex IV. These data support the idea that mitochondrial dysfunction appears to occur due to inhibition or modification of respiratory complex rather than deletions of mitochondrial DNA. Indeed, these changes were seen in the stratum radiatum where synaptic pathology is readily detected, indicating that mitochondrial function is impaired and could potentially contribute to or even initiate the synaptic pathology in prion disease. ***(Am J Pathol 2010, 177:1411–1421; DOI: 10.2353/ajpath.2010.091037)***

Mitochondria are vital organelles in all eukaryotic cells and are responsible for the efficient generation of high-energy compounds such as ATP produced by oxidative-phosphorylation system, also called the respiratory chain. The mitochondrial respiratory chain is located in the inner mitochondrial membrane and consists of five complexes (complexes I–V), each consisting of multiple subunits encoded by both nuclear and mitochondrial DNA (mtDNA), except complex II or succinate dehydrogenase (SDH) that is entirely encoded by nuclear DNA.[1] Cytochrome c oxidase (COX) or complex IV is the final component of the respiratory chain complex crucial for ATP production and the site of the highest oxygen consumption.[2] Neuronal mitochondria display considerable morphological uniformity particularly in terms of the folding of the energy-transducing inner membrane,[3] which forms numerous invaginations or cristae. Within the neuron, the synaptic compartment is the site at which demands on mitochondrial functions, such as energy supply and buffering of intracellular Ca^{2+} are especially significant.[4,5] The interdependence of synaptic activity and mitochondrial distribution has been described both at the presynaptic[6] and the postsynaptic elements of dendritic spines of living hippocampal neurons.[7]

Several neurodegenerative diseases in which there is accumulation of misfolded proteins, for example Alzheimer's disease and Parkinson's disease,[8–10] are associated with malfunction of both mitochondria and synaptic compartments. Malfunctions of mitochondrial metabolism that lead to reduced ATP production, impaired Ca^{2+} buffering and generation of reactive oxygen species may contribute to both aging and neurodegenerative disease.[11] The inner-membrane structural alterations, in particular numerous dilated or swollen cristae have been

Supported by UK Medical Research Council (MRC) grant G0501636.

Accepted for publication May 6, 2010.

CME Disclosure: None of the authors disclosed any relevant financial relationships.

Address reprint requests to Zuzana Sisková, MSc, Ph.D.; CNS Inflammation Group, School of Biological Sciences, Mailpoint 840, LD80B, South Lab and Path Block, Southampton General Hospital, Southampton, SO16 6YD. E-mail: z.siskova@soton.ac.uk.

consistently implicated in processes associated with apoptosis and as a response to oxidative stress in various neurodegenerative diseases.[8,12]

Prion diseases are fatal transmissible neurodegenerative diseases that affect several species, including humans. The pathological features of prion diseases are extensive neuronal loss, vacuolation, synaptic alterations, and accumulation of a misfolded and protease-resistant form of the prion protein, commonly termed PrP^{Sc}.[13] There is evidence that in murine prion disease synaptic and dendritic alterations precede neuronal death,[14–18] however, the role of the mitochondria in these early synaptic changes has not been investigated during disease evolution.

We hypothesized that mitochondrial abnormalities could accompany or perhaps contribute to early synaptic changes in the ME7 model, a murine model that we have previously characterized in some detail.[15,17–18] In the present study we demonstrate that the activity of respiratory complex IV is significantly decreased in the hippocampus of diseased animals. This contrasts with the sustained expression of porin, a voltage-gated anion channel located in the outer mitochondrial membrane that is widely used as a mitochondrial marker, and sustained expression of functionally important subunits of complex IV and complex II. Further, morphometric data suggest that mitochondrial numeric density remained unchanged. Interestingly, these changes correlated both temporally and spatially with early loss of Type I (excitatory) synapses in the stratum radiatum. The role of mitochondria is extensively studied as a primary cause of neuronal cell death or as a secondary phenomenon occurring on the way to neuronal death. The current study used tractable, staged and well-characterized prion pathology of the ME7 model that supports the role of an early dysfunction, which thus could be a contributor to disease progression rather than simply a consequence.

Materials and Methods

Animals

C57BL/6J female mice ages 8 to 10 weeks were obtained from Harlan Laboratories (Bicester, UK) and were group-housed within the animal care facilities in the School of Biological Sciences, University of Southampton as described previously.[18]

Surgeries

All operations were performed under the UK Home Office license, as described previously.[18] Briefly, surgery was performed when the mice were 11 to 12 weeks old. Mice were anesthetized by intraperitoneal injection of Avertin (2,2,2-tribromoethanol solution) (20 ml/kg) and mounted in a stereotaxic frame (David Kopf Instruments, Tujunga, CA). Injections of 1 μl of homogenate (10% w/v in sterile PBS) of either normal C57 mouse brain (NBH-animals) or of a ME7 prion agent-infected brain (ME7-animals) were made bilaterally into the dorsal hippocampus with a 10-μl Hamilton syringe. The suspension was slowly infused and the needle was left in place for 2 minutes before being slowly withdrawn. Mice were placed in a heated recovery chamber and when fully recovered, rehoused in groups and checked daily. Extracted tissue was analyzed using various techniques as described below at early stages (10 and 12 weeks p.i.) and at late stages (16, 18, and 20 weeks p.i.).

Electron Microscopy

Tissue Preparation

NBH- and ME7-animals were terminally anesthetized with sodium pentobarbital and sacrificed by perfusion fixation for transmission electron microscopy at 10, 12, 16 and 18 weeks post injection (p.i.) as described previously.[18] A slow cardiac perfusion (20 to 30 minutes) was performed with fixative containing 3.4% paraformaldehyde, 1.25% glutaraldehyde, and 0.2% picric acid in 0.1 mol/L sodium phosphate buffer (final pH 7.2 to 7.4) immediately after short ($<$1.5 minutes) perfusion with heparinized saline, to minimize synaptic and glial ultrastructural changes that could be caused by brain hypoxia. The optimal perfusion fixation protocol was established by carefully monitoring ultrastructural preservation of synaptic vesicle integrity, post-synaptic density and mitochondrial ultrastructure in NBH- and naive animals to ensure that the observed abnormalities are disease-associated. After approximately 1 hour, the brains were dissected and postfixed in fresh fixative overnight at 4°C, and 150 μm thick coronal sections were cut on a vibrotome and the area of CA1 pyramidal layer and stratum radiatum was dissected out. Microdissected areas were washed in 0.1 mol/L sodium phosphate buffer and postfixed at room temperature for 1 hour in 1% osmium tetroxide. Tissue blocks were dehydrated at room temperature through graded ethanols to 100% for 10 minutes each, including 1% uranyl acetate in 70% ethanol for 40 minutes. Blocks were placed in acetonitrile for 10 minutes and overnight in a 50:50 solution of acetonitrile:TAAB resin, subsequently infiltrated with fresh TAAB resin for 6 hours and polymerized at 60°C for 20 to 24 hours. TAAB blocks were hand trimmed, followed by glass trimming at room temperature to a trapezoid containing CA1 pyramidal cell bodies and dendritic arbor of stratum radiatum. Semithin (0.5 to 1 μm) sections were stained (1% v/v toluidine blue in 1% w/v borax) and used to guide further cutting of the specimen block to ultra-thin sections (60 to 70 nm). Ultra-thin sections were placed either onto thin bar mesh copper palladium grids or formvar-coated slot grids and stained in Reynolds lead stain for 5 minutes. The grids were then gently immersed three times in distilled water and left to dry. Grids were examined using a Hitachi H7000 transmission electron microscope with a MegaView III digital camera (Soft Imaging System) and subsequently processed using Adobe Photoshop software.

Electron Microscopy of Neuronal Mitochondria within the Stratum Radiatum

Mitochondrial Area Measurements

Measurements were generated from transmission electron microscopy images with a magnification of ×20,000; images were taken from at least two sections of a minimum of 10 sections apart within the tissue block and were positioned to avoid blood vessels, occasional areas of myelination, and the astroglial swelling to ensure that predominantly, if not exclusively, neuronal mitochondria were analyzed. ImageJ software was used to calculate the area by drawing around of each individual mitochondrion analyzed. At least 100 measurements for each animal were generated at 10 ($n = 6$), 12 ($n = 3$), 16 ($n = 3$), and 18 ($n = 3$) weeks p.i. for both NBH- and ME7-animals.

Mitochondrial Density Measurements

Measurements were generated from at least two images at magnification of ×3000 taken from 2 sections at least 10 sections apart within the tissue block from each animal, every mitochondria visible by eye was marked with a dot within a counting frame of 286 μm^2 positioned to avoid blood vessels, occasional areas of myelination, and the astroglial swelling. To ensure that only neuronal mitochondria were included the defining ultrastructural criteria used for identification of astrocytes and neuronal cells were applied as described previously.[18]

Briefly, astrocytes in comparison with neurons are characterized as cells whose cytoplasm is generally electron lucent or pale. The most prominent cytoplasmic component of the astrocyte is the numerous fibrils or filaments that occur throughout the perikaryon and extend as parallel arrays into the processes, the filaments are 8 to 9 nm in diameter (generally smaller than the neurofilaments). In contrast to neurofilaments, they commonly occur in closely packed bundles. Another prominent difference is the sparse presence of organelles in the cytoplasm of astrocytes; the organelles are mainly confined to the perikaryal region, the mitochondria are generally elongated and in the processes they are usually oriented parallel to the long axes of the processes and parallel to the filaments.

Quantification of Ultrastructural Defects

Quantification of mitochondrial ultrastructural defects was performed from identical images used for the area measurements as indicated above. Every mitochondria of neuronal origin was analyzed and based on its ultrastructural appearance classified into one of following categories: intact mitochondria with normal appearing cristae (Type I); abnormal mitochondria with either swollen, irregular, or whorling cristae (Type II); mitochondria with discontinuous outer membrane or deficient cristae (Type III); and mitochondria with both swollen and deficient cristae or both discontinuous outer membrane and swollen cristae (Type IV) (for further details see *Results*). At least 75 mitochondria were analyzed for each animal at 10 ($n = 3$), 12 ($n = 3$), 16 ($n = 3$), and 18 ($n = 3$) weeks p.i. for both NBH- and ME7-animals, raw data per individual animal have been expressed as percentage of total number of mitochondria analyzed. The quantification was performed blinded and the identities of the sections and images were only revealed to the observer after the data analysis was complete.

Immunohistochemistry

Coronal hippocampal sections (10 μm) were cut from formalin-fixed, paraffin-embedded brains, prepared as described previously,[19] the tissue was processed for immunohistochemistry following citrate buffer and microwave antigen retrieval. Nonspecific peroxidase activity was eliminated by incubating sections in 1 ml H_2O_2/100 ml ethanol (1% H_2O_2) for 10 minutes. Sections were incubated in a humid chamber for 90 minutes at room temperature with the primary antibody, a mouse monoclonal to porin (human mitochondrial) (1:300; Invitrogen, Paisley, UK, Molecular Probes). The mouse-on-mouse kit (Vector Laboratories, Inc., Peterborough, UK) was used according to the manufacturer's instructions to minimize any background staining. Sections were then incubated with avidin-biotin complex (Vector Laboratories, Inc.): 0.05% diaminobenzidine hydrochloride was used as substrate in the peroxidase reaction. Sections were counterstained with hematoxylin and dehydrated before mounting in Depex.

Histochemistry (Complex IV Activity)

The complex IV activity was detected as described previously.[20] Fresh frozen coronal sections through the dorsal hippocampus (8 μm) were air dried for 30 minutes at room temperature before incubation in COX medium (100 mmol/L cytochrome c, 4 mmol/L diaminobenzidine tetrahydrochloride, and 20 mg/ml catalase in 0.2 mol/L phosphate buffer, pH 7.0) at 37°C for 50 minutes. To detect mitochondria that lack complex IV activity, the activity of complex II, which would be unaffected by any mtDNA deletions, was determined by incubating in succinate dehydrogenase medium (130 mmol/L sodium succinate, 200 mmol/L phenazine methosulphate, 1 mmol/L sodium azide, 1.5 mmol/L nitroblue tetrazolium in 0.2 mol/L phosphate buffer, pH 7.0) at 37°C for 40 minutes immediately following the incubation in COX medium and washing steps. Following histochemistry, the sections were dehydrated followed by Histoclear and mounted in Depex.

The density of staining corresponding to complex IV activity was determined by monochrome pixel density analysis of digitally captured images using ImageJ software (U.S. National Institutes of Health, *http://rsb.info.nih.gov/ij/download.html*, last accessed July 8, 2010).

Uniformly stained areas of stratum radiatum in the hippocampus (avoiding unstained areas such as blood vessels) and subgranular layers of lateral parietal associated cortex were selected and density measurements

were performed as described previously.[15] The transmittance of the stratum radiatum was expressed as a ratio relative to the transmittance in the lateral parietal cortex (layers IV–VI). At least four measurements obtained from four different sections were included from at least three animals per experimental group.

Complex IV activity in relation to mitochondrial proteins expression in fresh frozen sections was determined using a recently described novel method.[21] In brief, the complex IV histochemistry was performed as described above: then immunocytochemistry with primary antibodies binding to porin or subunits of complex IV [subunit-I (COX-I) and subunit-II (COX-II)] and complex II (70 kDa) (Cambridge Biosciences, Cambridge, UK) using the Menapath X-cell Plus HRP Polmyer detection system (A. Menari Diagonsitics, Wokingham, UK) with Vector SG (gray precipitate) as the chromogen was performed on the same section. Sections were dehydrated and mounted as usual. Bright field images of the two chromogens diaminobenzidine and Vector SG were obtained using tuneable filters to acquire multispectral images (Nuance imaging, CRi imaging, Woburn, CA). Deconvolution methods were then used to unmix the two images, which can then be quantified and pseudocolored.[21]

Dissection of Hippocampus

All dissection procedures were performed at 4°C. The hippocampal formation was dissected out, and placed on dry ice. Samples for biochemical analyses were homogenized in suspension buffer (2% SDS/25 mmol/L HEPES/125 mmol/L KCL containing a mixture of phosphatase inhibitors and Complete protease inhibitor cocktail (Roche, UK). Samples were incubated on ice for 1 hour then centrifuged at 15,000 rpm for 30 minutes at 20°C. The supernatant was collected as the SDS soluble fraction. Proteins were quantified using the Bio-Rad protein assay (Bio-Rad, Hercules, CA), solubilized in loading buffer and analyzed by SDS-polyacrylamide gel electrophoresis and Western blotting according to standard protocols.[22] The hippocampal CA1 subregions used in mtDNA studies were microdissected and stored at −80°C before DNA extraction.

Western Blot Procedure

Membranes were blocked in 5% nonfat milk for 1 hour at room temperature and then incubated in Tris-buffered saline containing 0.1% Tween-20 and monoclonal antibody against porin protein (1:4000; Invitrogen, Molecular Probes). Membranes were incubated with the primary antibody overnight at 4°C. The blots were washed and incubated for 1 hour with fluorescently labeled anti-mouse secondary antibody at room temperature. Protein band intensities were analyzed using a LiCor Odyssey infrared detection system following the manufacturer's guidelines, and normalized to total protein loading as previously described.[17]

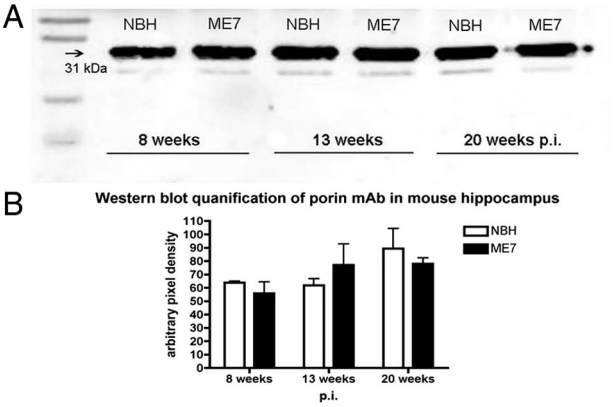

Figure 1. A: Western blot analysis of samples from dissected hippocampal tissue from NBH- and ME7-animals at different stages of disease illustrate the expression of porin protein (31-kDa band), a mitochondrial-specific protein located in the outer mitochondrial membrane. **B:** Quantification of porin expression (n = 4/time point) in ME7-animals and age-matched NBH-animals where porin levels are expressed relative to the total protein loaded onto the gel and assayed by Licor Odessey detection system. No statistically significant differences have been detected (two-way analysis of variance, Bonferroni post-tests).

Statistical Analysis

The identities of the sections, images and samples were only revealed to the observer after the data analysis was complete. Raw data accumulated from every block were collated using Microsoft Excel and appropriate statistical tests were applied (indicated in *Results* section) to compare final data between NBH- and ME7-animals using Graph Pad Prism 4.0 (Graph Pad Software Inc., San Diego, CA).

Results

The loss of synapses from the stratum radiatum of the hippocampus is an early feature of the neuropathology in experimental prion diseases, and precedes neuronal loss.[14,15,17] To detect possible changes in mitochondrial density we used three different methods of analyzing hippocampal tissue samples, a structure in which the synaptic loss has already been documented, and compared them with age-matched NBH-animals. Western blot analysis of samples from dissected hippocampus (n = 4 animals/time point) (Figure 1A and B; Two-way analysis of variance, Bonferroni posttests) revealed that expression of porin protein, a mitochondrial outer membrane marker, did not change significantly during disease progression. Immunocytochemistry on brain sections passing through the dorsal hippocampus of NBH- and ME7-animals (n = 3 animals/time point) (Figure 2A) for porin yielded no evidence of reduced mitochondrial density consistent with the data from Western blots. However, changes of the distribution of the porin protein were apparent. For example, in NHB-animals the levels of porin expression in the stratum oriens and the most proximal stratum radiatum were denser than porin expression in the stratum radiatum of the distal CA1 dendrites. This differential laminar pattern was lost in both early (ME7 ES) and late stage (ME7 LS) ME7-animals (Figure 2A). A

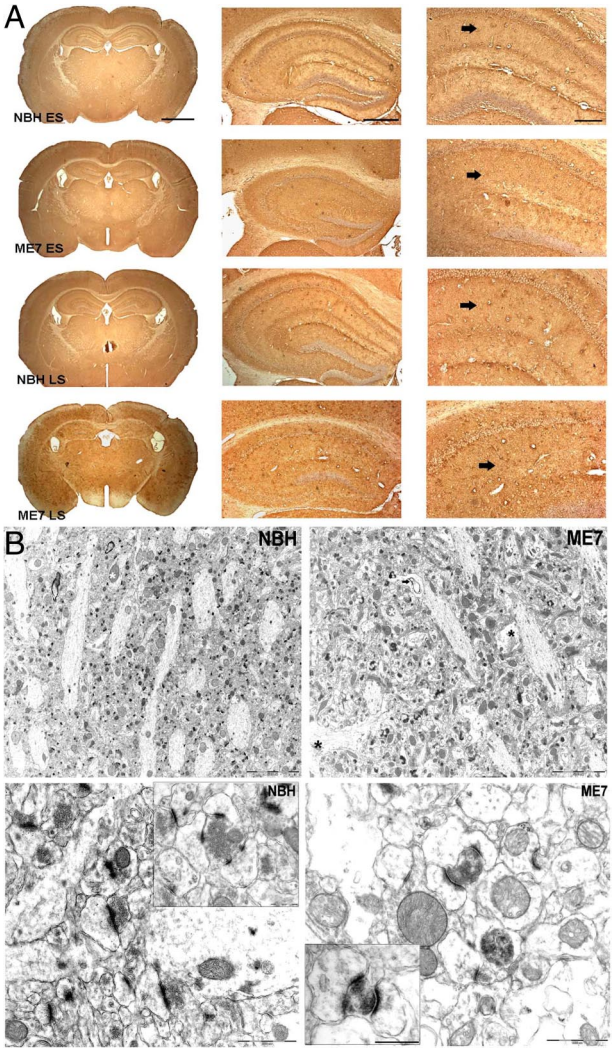

Figure 2. A: Immunohistochemistry of fixed-brain sections reveals distribution and expression of porin in the neuropil of the stratum radiatum (**arrows**) in both NBH- and ME7-animals. ES (early stage = 12 to 13 weeks p.i.), LS (late stage = 19 weeks p.i.). Note the vacuolation and shrinkage of the hippocampus in ME7-animals. Scale bars: 1.5 mm (first panel), 500 μm (second panel), and 200 μm (third panel). **B: Upper panel:** electron micrographs of the stratum radiatum neuropil illustrating mitochondrial population in NBH- and ME7-animals at 18 weeks p.i. Examples of neuronal mitochondria included in analysis are labeled by **white asterisks** and mitochondria in non-neuronal cells by **black asterisks**, specifically in swollen astrocytic processes (see *Results* for detailed description) in ME7 tissue. Note the presence of whorling membrane fragments (**arrow**), frequently associated with spongiform vacuolization in ME7-animals. Scale bars = 5 μm. **Lower panel:** electron micrographs of the stratum radiatum neuropil illustrating Type I (excitatory) synapses in NBH-animals and ME7-animals at 16 weeks p.i. . Alterations of the synaptic morphology are evident in ME7-animals; presynaptic terminals are filled with electron-dense cytoplasm, although still visible, structurally compromised synaptic terminals are being enwrapped by curved postsynaptic density specialization. Scale bars = 1 μm; 0.5 μm (**insets**).

progressive atrophy of the hippocampus, mainly affecting the pyramidal cell and the stratum radiatum layers was also observed in diseased tissue[15] (Figure 2A).

We next analyzed the mitochondrial density within the neuronal processes of the stratum radiatum as illustrated in Figure 2B (upper panel). We have previously described extensive and selective loss of Type I (excitatory) synapses in the hippocampus,[18] and from 12 weeks p.i. and onwards dark degenerating synapses were present

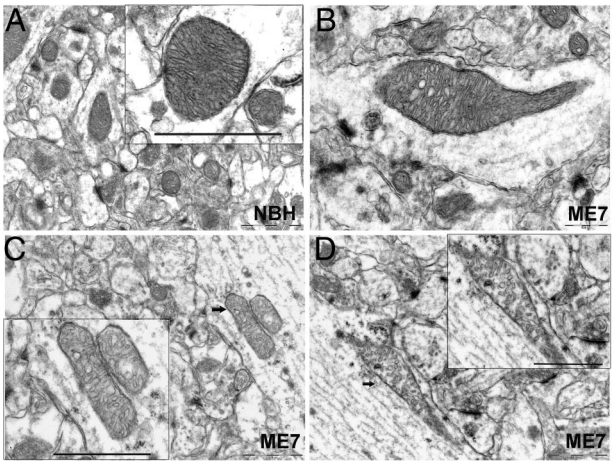

Figure 3. Stratum radiatum neuropil, electron micrographs illustrating mitochondrial morphology in NBH-animals (**A**, Type I) at 18 weeks p.i. and representative examples of mitochondria with abnormal morphology that frequently appeared in ME7 animals at 16 (**B**, Type II) and 18 weeks (**C**, Type III; **D**, Type IV) p.i. Scale bars: 1 μm (**A**); 0.5 μm (**B**); 1 μm (**C, D**); and 1 μm (all **insets**). **Arrows** indicate the location of the images shown in the corresponding **insets**.

in ME7-animals that were not detected in NBH-animals (Figure 2B lower panel). In agreement with previous studies, mitochondria were rarely found in dendritic spines;[23] approximately 10% of all presynaptic elements in the CA1 region contained a mitochondrion both in NBH- and ME7-animals. Among many hundreds of degenerating synaptic boutons from 12 weeks onwards we have not detected a mitochondrion present in the degenerating terminal while its individual elements could still be resolved.[18] These observations make it unlikely that the mitochondria from the presynaptic elements degenerate together with the synapses.

Although mitochondria are sparse within the hippocampal astrocytic processes, the criteria used previously for identification of astrocytes and neuronal cells[18] were applied to ensure that predominantly, if not exclusively, neuronal mitochondria were included. As disease progressed we observed a pronounced heterogeneity in the mitochondrial morphology and the morphology of the cristae in particular in all ME7-animals (Figure 3). In neuronal processes, mitochondria appeared usually as rodlets about 0.1 micron across and 1 micron long containing longitudinally oriented, densely packed cristae. In the few presynaptic terminals where we did detect mitochondria, they were small and globular in shape. Mitochondria with both normal and abnormal ultrastructural appearance were present in diseased tissue and we characterized them as follows: Type I - normal appearing mitochondria with mostly longitudinally oriented and tightly packed cristae (Figure 3A); Type II - abnormal mitochondria with either swollen, irregular, or whorling cristae in which the characteristic longitudinal orientation and/or the tight and regular spacing of cristae were lost or severely compromised (Figure 3B). At latter stages of the disease we have detected increasing numbers of mitochondria with a discontinuous outer membrane or deficient cristae, in which the cristae order was distorted by holes with an empty matrix—Type III (Figure 3C). Finally, some mitochondria with swollen and deficient

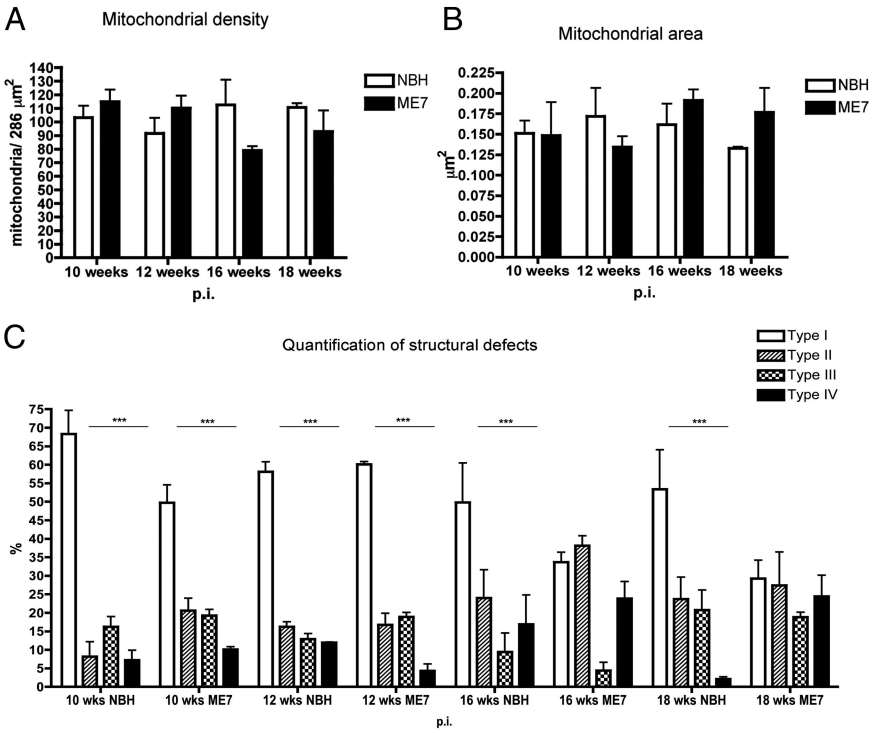

Figure 4. **A:** Quantification of mitochondrial density in neuronal processes of the stratum radiatum of NBH- and ME7-animals. No statistically significant differences have been detected ($P = 0.0819$, two-way analysis of variance, Bonferroni post-tests). **B:** Quantification of mean mitochondrial area in neuronal population of the stratum radiatum (at least 100 mitochondria analyzed per animal [minimum $n = 3$/time point], two-way analysis of variance, Bonferroni post-tests). **C:** Quantification of mitochondrial structural defects in neuronal population of the stratum radiatum in ME7- and NBH-animals (for a more detailed description of the identification criteria see *Results*). Percentages of intact mitochondria with normal appearing cristae (Type I); abnormal mitochondria with either swollen, irregular or whorling cristae (Type II); mitochondria with discontinuous outer membrane or deficient cristae (Type III); and mitochondria with both swollen and deficient cristae or both discontinues outer membrane and swollen cristae (Type IV) have been expressed from total pool of all neuronal mitochondria in NBH- and ME7-animals against disease stage ($^*P < 0.05$, $^{**}P < 0.01$, $^{***}P < 0.005$; two-way analysis of variance, Bonferroni post-tests).

cristae, or swollen cristae and discontinuous outer membrane, Type IV, were present (Figure 3D).

Despite the frequent morphological abnormalities, the density of neuronal mitochondria per unit area in the stratum radiatum analyzed from electron micrographs at 10, 12, 16, and 18 weeks p.i. (Figure 4A) did not show any significant changes (two-way analysis of variance, Bonferroni post-tests). This ultrastructural quantitative method confirmed our initial observations described above (Figures 1 and 2A); not only were the mitochondrial counts similar in NBH-animals and at the onset of synaptic loss (12 weeks p.i.) in ME7-animals, but surprisingly the density was not significantly different at later stages in ME7-animals (16 to 18 weeks p.i.).[18]

Ultrastructural integrity is a key indicator of mitochondrial function[24] and mitochondrial swelling, generally reflected by an increase of the mitochondrial area is a well-accepted hallmark of dysfunction of this organelle.[8,25] The mitochondrial area of at least 100 neuronal mitochondria from the stratum radiatum (minimum $n = 3$ animal/time point) was measured. To achieve the best representation possible, the same animals and sections were used as in density analysis described above. Throughout disease progression no statistically significant differences in mitochondrial area between NBH- and ME7-animals were observed (Figure 4B; two-way analysis of variance, Bonferroni post-tests), although at 18 weeks p.i. there is a trend for an increase of the area in ME7-animals.

We next quantified the frequency of mitochondria with ultrastructural changes in the inner membranes that we described above. In NBH-animals the Type I mitochondria (intact mitochondria with normal appearing cristae) were predominantly represented; their percentage was always significantly higher than any other types (Type II–IV) (Figure 4C). In contrast to this, the proportions of Type II–IV mitochondria (mitochondria with structural abnormalities) increased considerably at later stages (16 and 18 weeks p.i.) in all ME7-animals. In fact, when compared with early stages (10 and 12 weeks p.i.) and NBH-animals, individual categories of these abnormal mitochondria were no longer significantly different from the pool of intact, normal appearing (Type I) mitochondria (Figure 4C; two-way analysis of variance, Bonferroni post-tests).

The findings described above provide evidence that the mitochondrial inner membrane is ultrastructurally compromised during the progression of prion disease. We next wished to establish whether these changes are reflected in the functional activity of the respiratory chain complexes. We stained frozen tissue sections using enzyme histochemistry for COX (complex IV) and SDH (complex II) activity, a widely used method for studying mitochondrial function in other pathological and neuropathological conditions, including Alzheimer's disease.[20,26,27,28] The pattern of the complex IV functional activity in the control brains revealed a laminar distribution in the hippocampus, similar but not identical to the distribution of porin protein. The levels of activity were predominantly concentrated in the stratum oriens, lacunosum moleculare layer, and in the most proximal and distal parts of the CA1 dendrites in the stratum radiatum and in the CA3 area. The assay indicated a decline in functional activity of complex IV in the dorsal hippocampus of all ME7-animals at 12 weeks p.i. (Figure 5, A and B) that persisted in late stage of the disease ($n = 4$ animals/time point) (Figure 5, A and C).

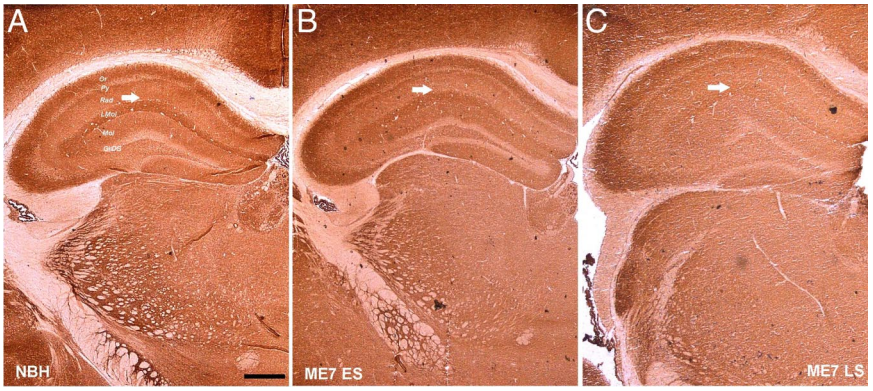

Figure 5. Cytochrome c oxidase activity in fresh coronal brain sections of a NBH (**A**); ME7 ES (early stage = 12 to 13 weeks p.i.; **B**) and ME7 LS (late stage = 19 weeks p.i.; **C**) animals; Hippocampal layers: Or-oriens, Py-pyramidal Cell, Rad-stratum radiatum; LMol-lacunosum moleculare layer; dentate gyrus layers: Mol-molecular, GrDG-granular layer. Scale bar = 100 μm. Note progressive loss of the distinct laminar pattern (**arrows**, Rad and LMol layers) of COX IV activity in the hippocampal formation of ME7-animals.

On closer examination we observed that the laminar distribution of the activity was altered, it was apparent that in the CA1 pyramidal layer, the stratum radiatum and the lacunosum moleculare layer of the hippocampus there was a reduction in the intensity of the product deposited due to the COX enzymatic reaction (Figure 6, A–C). The CA3 area appeared to be unaffected at 12 weeks p.i. and maintained relatively high activity levels even at the late stage when compared with other areas within the hippocampus. We did not detect any blue (COX-deficient, complex II or SDH-positive) elements either within the pyramidal layer or the stratum radiatum even in the late disease stage (Figure 6D). These findings would suggest that the COX activity is reduced as quantified by densitometry (Figure 6E; $P < 0.001$ one-way analysis of variance, Bonferroni post-tests) rather than completely absent in ME7-animals and therefore does not allow for generation of the blue product generally observed in COX-deficient cells.

To further clarify whether the early alterations in COX activity result from local mitochondrial loss of activity we took advantage of a recently described method that allowed us to assay and co-localize the COX activity in relation to expression of mitochondrial proteins such as porin and subunits of complex IV and complex II in the same tissue section.[21] Fresh frozen hippocampal sections from a control animal were stained consecutively (Figure 7, A–D) for COX activity and mitochondrial proteins. The activity was detected in neurons in CA1 and in the adjacent neuropil in the stratum radiatum (brown in A, pseudocoloured red in C). The porin expression (gray in A, pseudocoloured green in D) almost completely overlaps with the COX activity pattern as seen in the merged image in Figure 7B. In contrast to this, sections from a ME7-animal at 12 weeks p.i. (Figure 7, E–H) indicated selective loss of COX activity in neurons and neuropil (brown in E, pseudocoloured red in G) but comparable levels of porin-positive mitochondria (gray in E, pseudocoloured green in H) to NBH-animals (D). The merge of images G and H (Figure 7F) reveals porin positive mitochondria lacking COX activity. When quantified using densitometry (Figure 7I), statistical analysis confirmed a significant decline of COX activity both at early (12 weeks p.i.) and late stage (18 weeks p.i.) that occurs independently of mitochondrial loss ($P < 0.001$, one-way analysis of variance, Bonferroni post-tests). As not all mitochondria labeled with porin showed COX activity, we determined activity relative to immunoreactivity of individual

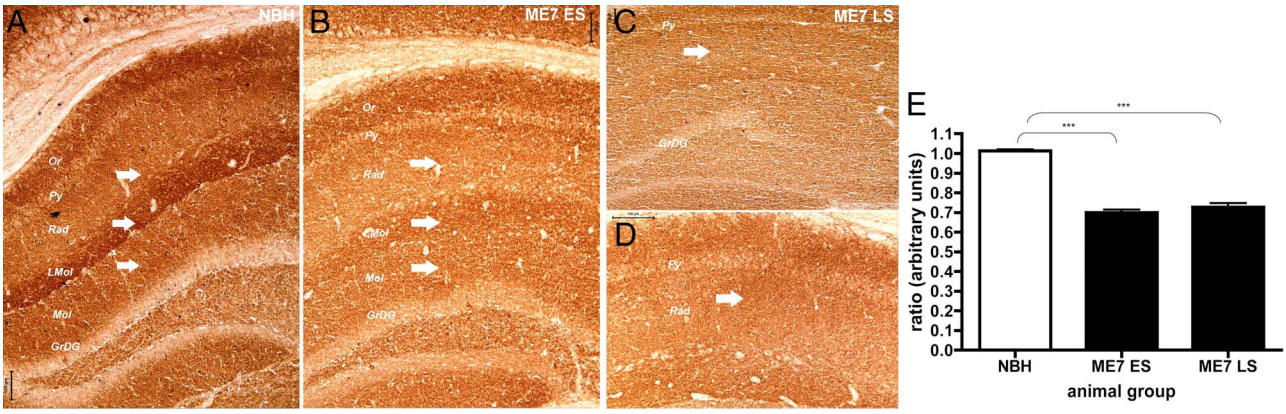

Figure 6. **A:** Cytochrome c oxidase activity in fresh coronal brain sections of a NBH-animal at 18 weeks p.i.; (**B**) ME7 ES (ME7-animal, early stage = 12 to 13 weeks p.i.); and (**C**) ME7 LS (ME7-animal, late stage = 19 weeks p.i.). **D:** The absence of respiratory-deficient cells which would appear blue (COX-deficient, complex II or SDH-positive) was demonstrated by COX/SDH assay at the late stage of the disease 19 weeks p.i. Hippocampal layers: Or-oriens, Py-pyramidal cell, Rad-stratum radiatum; LMol-lacunosum moleculare layer; dentate gyrus layers: Mol-molecular, GrDG-granular layer. Scale bars = 100 μm. **E:** Changes in COX activity in the stratum radiatum of NBH- and ME7-injected animals. The graph plots the ratio of stratum radiatum staining to lateral parietal associated cortex staining against disease stage. Statistically significant reduction in the stratum radiatum of ME7 animals (*$P < 0.05$, **$P < 0.01$, ***$P < 0.005$; one-way analysis of variance, Bonferroni post-tests). Note that decrease of the COX activity (**arrows**, Rad, LMol, and Mol layers) correlates both spatially and temporally with initial pathology of synapses in the stratum radiatum.[17,18]

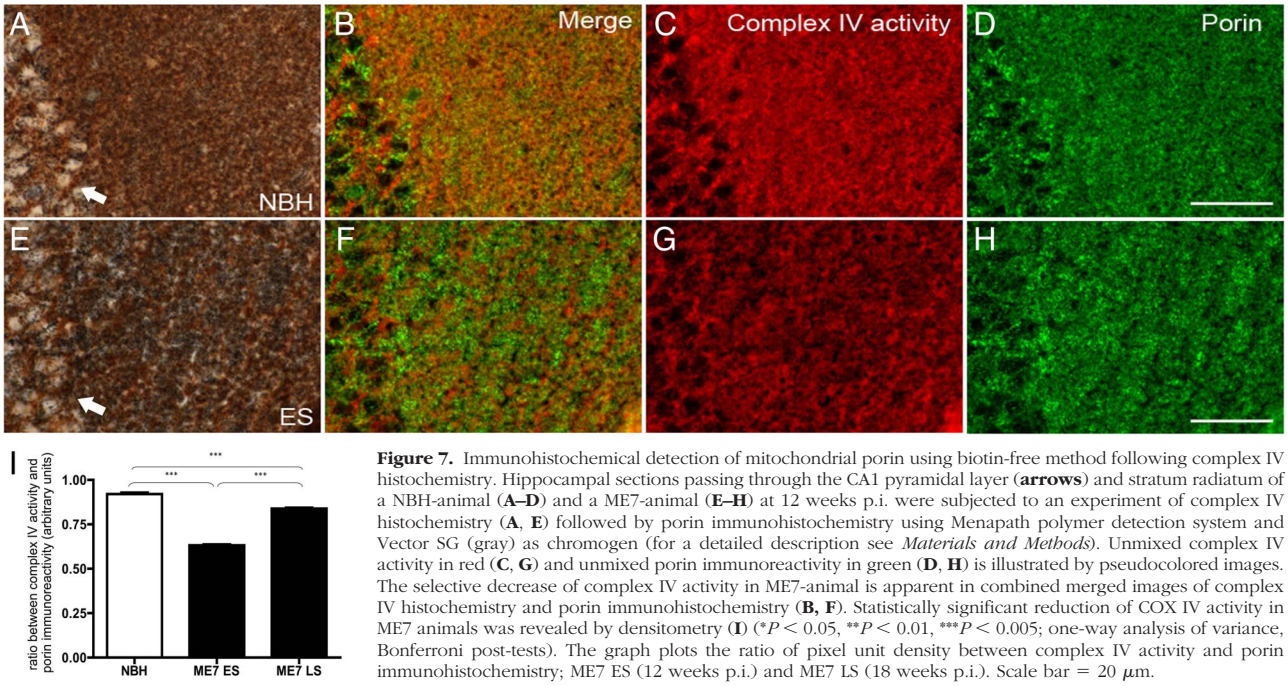

Figure 7. Immunohistochemical detection of mitochondrial porin using biotin-free method following complex IV histochemistry. Hippocampal sections passing through the CA1 pyramidal layer (**arrows**) and stratum radiatum of a NBH-animal (**A–D**) and a ME7-animal (**E–H**) at 12 weeks p.i. were subjected to an experiment of complex IV histochemistry (**A**, **E**) followed by porin immunohistochemistry using Menapath polymer detection system and Vector SG (gray) as chromogen (for a detailed description see *Materials and Methods*). Unmixed complex IV activity in red (**C**, **G**) and unmixed porin immunoreactivity in green (**D**, **H**) is illustrated by pseudocolored images. The selective decrease of complex IV activity in ME7-animal is apparent in combined merged images of complex IV histochemistry and porin immunohistochemistry (**B, F**). Statistically significant reduction of COX IV activity in ME7 animals was revealed by densitometry (**I**) (*$P < 0.05$, **$P < 0.01$, ***$P < 0.005$; one-way analysis of variance, Bonferroni post-tests). The graph plots the ratio of pixel unit density between complex IV activity and porin immunohistochemistry; ME7 ES (12 weeks p.i.) and ME7 LS (18 weeks p.i.). Scale bar = 20 μm.

catalytic subunits because mitochondrial dysfunction may be the result of modification, inhibition, or loss of catalytic subunits. We thus examined, using the same novel combined histochemical and immunocytochemistry technique, COX activity relative to catalytic subunits of complex IV and subunit II. Interestingly, when corrected for catalytic subunits of complex IV [subunit-I (COX-I) and subunit-II (COX-II), $P < 0.0001$ and $P = 0.0002$ respectively] and subunit of complex II (70 kDa) ($P = 0.0075$) or porin ($P < 0.0001$), the COX activity in diseased animals remained significantly reduced (one-way analysis of variance) (Table 1).

The accumulation of various mutations in the mitochondrial genome has been proposed as an important factor contributing to aging and neurodegeneration and could also underlie alteration of the COX activity.[29,30] We next screened mtDNA from microdissected CA1/stratum radiatum regions for possible deletions. Freshly microdissected tissue from six animals ($n = 3$/treatment group) at late stage (20 to 21 weeks p.i.) was used to isolate DNA for amplification by PCR; similarly as described previously.[31] No mtDNA deletions were detected on resolving the amplified PCR product from both NBH- and ME7-animals. A full-length fragment of 14.55 kb spanning the major arc of the mitochondrial genome has been detected as expected when no mtDNA deletions are present (data not shown).

Discussion

Synaptic loss is a common component of various neurodegenerative diseases including prion disease; however, the underlying mechanisms are not well understood. Damage to mitochondria and/or their dysfunction are frequently associated with these pathologies.[8–10] A possible mitochondrial contribution to the prion pathology has not been explored in any detail to date.

Our present study demonstrates that the regions of synaptic loss in murine prion disease contain neuronal

Table 1. Relationship between COX Activity and Immunoreactivity of Catalytic Subunits of Complex IV, Complex II (70 kd) and Porin Protein

		P value
ratio COX activity/Porin		
NBH	0.9208 ± 0.0104	<0.0001
ES	0.6323 ± 0.0064	
LS	0.8392 ± 0.0113	
ratio COX activity/COX I subunit		
NBH	0.9704 ± 0.0537	<0.0001
ES	0.2434 ± 0.0122	
LS	0.4759 ± 0.0290	
ratio COX activity/COX II subunit		
NBH	1.0640 ± 0.0789	0.0002
ES	0.7437 ± 0.0379	
LS	0.9362 ± 0.0413	
ratio COX activity/ Complex II (70 kd)		
NBH	0.5363 ± 0.1303	0.0075
ES	0.3346 ± 0.0230	
LS	0.4675 ± 0.0370	

COX activity relative to presence of mitochondria and catalytic subunits of complex IV [subunit-I (COX-I) and subunit-II (COX-II)], complex II and outer membrane marker (porin) was established by enzyme histochemistry combined with immunohistochemistry on same tissue section (for detailed description see *Materials and Methods*). The activity to protein ratio was resolved using Nuance CRi system, providing normalization across three distinct mitochondrial subcompartments. A reduction in ratio reflects a decrease in COX activity; no significant change in densitometric values of porin and individual subunits immunoreactivity was detected (*$P < 0.05$, **$P < 0.01$, ***$P < 0.005$; One-way ANOVA), ME7 ES (12 weeks p.i.) and ME7 LS (18 weeks p.i.).

processes with abnormalities of the mitochondrial inner membrane and mitochondria, in which the respiratory complex IV function is impaired. However, no concomitant reduction in the mitochondrial density has been detected in contrast to early loss of the type I synaptic density.[18] Three independent quantitative methods led us to conclude that no or a very minor, undetectable change in mitochondria density occurs before (10 weeks p.i.) or at the time of initiation of the synaptic pathology (12 weeks p.i.). No significant increase of the mitochondria with structural abnormalities was detected either when compared with NBH-animals (12 weeks p.i.). A profound neuronal loss occurs at late stage[14,15] and presumably also involves changes of absolute mitochondrial numbers. However, using our approaches we failed to detect any such decline in mitochondrial density. The likely explanation is that as the neurons atrophy and die, the mitochondrial density per unit volume of neuropil remains relatively constant.

In the CNS, dendritic spines, the predominant recipients of excitatory synaptic input are recognized as a distinct biochemical compartment sufficient to provide the capacity for signaling at individual synapses. In contrast to dendritic shafts, mitochondria are rarely observed within dendritic spines of cortical or hippocampal neurons: exceptions are restricted to large and complex spines ("thorny excrescences") of CA3 pyramidal neurons.[23,32] In agreement with these latter studies, we observed the majority of mitochondria within dendritic shafts and presynaptic terminals in NBH- and ME7-animals, and only on a very few occasions were mitochondria present in dendritic protrusions. The low frequency of dendritic spines containing mitochondria in electron microscope preparations is in accord with findings from cultured hippocampal neurons.[7] Several studies indicate that the mitochondrial and synaptic functions in neuronal cells are co-dependent and well be synchronized, mitochondria can relocate to the compartment in which the activity and energy demands increase.[6,7] One possibility is that the first abnormalities of synaptic function in ME7-animals[33] could result in a reduction in or silencing of the mitochondrial function in response to decreased respiratory demands and a subsequent retraction of mitochondria from degenerating synaptic terminal to the remaining axonal compartment. These observations would explain the absence of changes in the mitochondrial density at early stages.[18]

As disease progressed we have encountered increasing numbers of neuronal mitochondria containing various morphological defects in the inner membrane morphology. Sequential COX/SDH activity assay revealed that these structural defects were accompanied with functional impairment of the complex IV activity. There are several possibilities for the impairment of the respiratory function.

An altered organization of the inner mitochondrial membrane may results in change of the mtDNA copy number, as mtDNA nucleoids are anchored on the matrix side of the inner membrane. We however considered this possibility as unlikely due to no change in protein levels encoded by mtDNA and distributed in all mitochondrial subcompartments.

It is possible that a misfolded form of the PrP^C could interact with neuronal mitochondria in the neuropil and interfere with their function, in a similar manner to that reported in Alzheimer's disease and its animal model.[34] Both specific and non-specific interactions of the misfolded form could be influencing mitochondrial membrane properties and function via intermediates such as phospholipase A2 similar to Aβ peptides.[35] Aiken and colleagues showed that mitochondria purified from brains of scrapie-infected hamsters contained high infectivity titers.[36] However, unlike Aβ peptide that interacts with the mitochondria of Alzheimer's disease patients and transgenic mice, in this study prion protein failed to show a significant association with these mitochondrial fractions. In contrast, the mitochondrial localization of the cellular prion protein PrP^C has been implicated in neuronal apoptosis in aged transgenic mice overexpressing PrP^C.[37] Further research will be required to exclude the possibility that misfolded PrP^C does not directly interact with any mitochondrial protein or bind to its membrane nonspecifically.

On the other hand, astrogliosis as observed in a prion disease[38] can be accompanied by up-regulation of nitric oxide as in various other pathologies.[39,40] It is documented that nitric oxide is a potent mediator of brain damage and may directly impair mitochondrial function[41] by inhibiting the binding of oxygen to complex IV[42] and when over-expressed, may impair the activity of mitochondrial respiratory chain complexes I and IV.[43,44] The fact that the decrease in COX activity was still apparent when normalized by measuring immunoreactivity of the catalytic subunits indicates either inhibition or inactivation of the complex as the most likely mechanism of mitochondrial dysfunction. The decrease in ratios was not due to a significant increase in the densitometric values of mitochondrial proteins immunoreactivity (data not shown).

Although no significant increase in inducible-nitric oxide synthase has been detected in prion diseased brains,[45,46] we have shown that in early stage disease (12–13 weeks p.i.) there is a significant increase in neuronal-nitric oxide synthase in the hippocampus.[47] The increase in neuronal-nitric oxide synthase occurs in the stratum radiatum and declines in late disease stage consistent with the changes in COX activity that we report here. Thus the idea that nitric oxide could damage mitochondria in ME7-animals is justified. However, this could go a step further because an increase in neuronal-nitric oxide synthase has been shown to be directly associated with neuronal injury and loss of synapses.[48]

In contrast to progressive deterioration of the mitochondrial ultrastructure in neuronal population, we generally did not observe any similar changes in other cell types. Specifically, within astrocytic processes that are frequently observed in degenerating hippocampal neuropil, the sparsely distributed mitochondria appeared to be normal.

Reduced mitochondrial numbers and altered morphology of the inner mitochondrial membrane (loss of internal structure with poorly defined and sparse cristae) were

also observed in mice lacking PrP^C. Mitochondria in hippocampi of these normal appearing animals frequently looked swollen, having significantly larger diameters when compared with wild-type animals.[49] Similar to a previous study,[50] we also detected neuronal mitochondria with fewer, poorly defined and swollen cristae. The inner membrane ultrastructure is an important parameter used for determination of the mitochondrial respiration capacity and is also the site where the reactive oxygen species are constantly produced.[51]

As indicated by the morphology defects and the reduction in complex IV activity, the respiratory capacity of neuronal mitochondria in prion disease could be compromised early on and coincides with initiation of the synaptic loss. A misbalance in the reactive oxygen species levels, among other changes, could be induced and this could further exacerbate the ongoing pathology. Mitochondrial abnormalities at the onset of behavioral deficits in ME7-induced murine prion disease are further confirmed by the observation that N-acetyl aspartate levels, synthesized by neuronal mitochondria with intact metabolism,[52] are decreased in the thalamus and hippocampus, brain regions associated with early behavioral deficits.[53] Studies of respiration rate in PrP-null brain mitochondria have yielded contradictory observations: a complex I specific increase in superoxide formation has been reported[54] but normal mitochondrial respiration rate was detected by others.[55]

Mutations of the mitochondrial genome accumulating with age and in diseases such as cardiomyopathies or Parkinson's disease have been suggested to be the underlying cause.[26,56] We examined whether specific decrease of the COX activity could be rooted in alterations of the mitochondrial genome, despite the fact that the brain mitochondria have a relatively long half-life.[57] As expected, we found that the mtDNA from diseased animals was intact and we assume that it is not the underlying cause for functional abnormalities.

In conclusion, here we present observations that implicate an overt mitochondria dysfunction in early pathogenesis of the experimental murine prion disease that could contribute to the disease progression. The intriguing mechanisms underlying the impairment of the mitochondrial function that could trigger and/or exacerbate synaptic loss remain to be clarified.

Acknowledgments

We thank Richard Reynolds (School of Biological Sciences, Southampton) for technical support throughout and Hussein Al-Malki (School of Biological Sciences, Southampton) for help with tissue processing.

References

1. Taylor RW, Turnbull DM: Mitochondrial DNA mutations in human disease. Nat Rev Genet 2005, 6:389–402
2. DiMauro S, Schon EA: Mitochondrial respiratory-chain diseases. N Engl J Med 2003, 348:2656–2668
3. Perkins GA, Renken CW, Frey TG, Ellisman MH: Membrane architecture of mitochondria in neurons of the central nervous system. J Neurosci Res 2001, 66:857–865
4. Shepherd GM, Harris KM: Three-dimensional structure and composition of CA3–>CA1 axons in rat hippocampal slices: implications for presynaptic connectivity and compartmentalization. J Neurosci 1998, 18:8300–8310
5. Rowland KC, Irby NK, Spirou GA: Specialized synapse-associated structures within the calyx of Held. J Neurosci 2000, 20:9135–9144
6. Stowers RS, Megeath LJ, Gorska-Andrzejak J, Meinertzhagen IA, Schwarz TL: Axonal transport of mitochondria to synapses depends on milton, a novel Drosophila protein. Neuron 2002, 36:1063–1077
7. Li Z, Okamoto K, Hayashi Y, Sheng M: The importance of dendritic mitochondria in the morphogenesis and plasticity of spines and synapses. Cell 2004, 119:873–887
8. Trimmer PA, Swerdlow RH, Parks JK, Keeney P, Bennett JP, Jr., Miller SW, Davis RE, Parker WD, Jr.: Abnormal mitochondrial morphology in sporadic Parkinson's and Alzheimer's disease cybrid cell lines. Exp Neurol 2000, 162:37–50
9. Castellani R, Hirai K, Aliev G, Drew KL, Nunomura A, Takeda A, Cash AD, Obrenovich ME, Perry G, Smith MA: Role of mitochondrial dysfunction in Alzheimer's disease. J Neurosci Res 2002, 70:357–360
10. Dawson TM, Dawson VL: Molecular pathways of neurodegeneration in Parkinson's disease. Science 2003, 302:819–822
11. Beal MF: Mitochondria take center stage in aging and neurodegeneration. Ann Neurol 2005, 58:495–505
12. Mannella CA: Structural diversity of mitochondria: functional implications. Ann NY Acad Sci 2008, 1147:171–179
13. Prusiner SB: The prion diseases. Brain Pathol 1998, 8:499–513
14. Jeffrey M, Halliday WG, Bell J, Johnston AR, MacLeod NK, Ingham C, Sayers AR, Brown DA, Fraser JR: Synapse loss associated with abnormal PrP precedes neuronal degeneration in the scrapie-infected murine hippocampus. Neuropathol Appl Neurobiol 2000, 26:41–54
15. Cunningham C, Deacon R, Wells H, Boche D, Waters S, Diniz CP, Scott H, Rawlins JN, Perry VH: Synaptic changes characterize early behavioural signs in the ME7 model of murine prion disease. Eur J Neurosci 2003, 17:2147–2155
16. Fuhrmann M, Mitteregger G, Kretzschmar H, Herms J: Dendritic pathology in prion disease starts at the synaptic spine. J Neurosci 2007, 27:6224–6233
17. Gray BC, Siskova Z, Perry VH, O'Connor V: Selective presynaptic degeneration in the synaptopathy associated with ME7-induced hippocampal pathology. Neurobiol Dis 2009, 35:63–74
18. Siskova Z, Page A, O'Connor V, Perry VH: Degenerating synaptic boutons in prion disease. Microglia activation without synaptic stripping. Am J Pathol 2009, 175:1610–1621
19. Cunningham C, Deacon RM, Chan K, Boche D, Rawlins JN, Perry VH: Neuropathologically distinct prion strains give rise to similar temporal profiles of behavioral deficits. Neurobiol Dis 2005, 18:258–269
20. Mahad D, Ziabreva I, Lassmann H, Turnbull D: Mitochondrial defects in acute multiple sclerosis lesions. Brain 2008, 131:1722–1735
21. Mahad DJ, Ziabreva I, Campbell G, Laulund F, Murphy JL, Reeve AK, Greaves L, Smith KJ, Turnbull DM: Detection of cytochrome c oxidase activity and mitochondrial proteins in single cells. J Neurosci Methods 2009, 184:310–319
22. Asuni AA, Cunningham C, Vigneswaran P, Perry VH, O'Connor V: Unaltered SNARE complex formation in an in vivo model of prion disease. Brain Res 2008, 1233:1–7
23. Bourne JN, Harris KM: Balancing structure and function at hippocampal dendritic spines. Annu Rev Neurosci 2008, 31:47–67
24. Mattson MP, Gleichmann M, Cheng A: Mitochondria in neuroplasticity and neurological disorders. Neuron 2008, 60:748–766
25. Witter RF, Watson ML, Cottone MA: Morphology and ATP-ase of isolated mitochondria. J Biophys Biochem Cytol 1955, 1:127–138
26. Arbustini E, Diegoli M, Fasani R, Grasso M, Morbini P, Banchieri N, Bellini O, Dal Bello B, Pilotto A, Magrini G, Campana C, Fortina P, Gavazzi A, Narula J, Vigano M: Mitochondrial DNA mutations and mitochondrial abnormalities in dilated cardiomyopathy. Am J Pathol 1998, 153:1501–1510
27. Old SL, Johnson MA: Methods of microphotometric assay of succinate dehydrogenase and cytochrome c oxidase activities for use on human skeletal muscle. Histochem J 1989, 21:545–555
28. Cottrell DA, Borthwick GM, Johnson MA, Ince PG, Turnbull DM: The

role of cytochrome c oxidase deficient hippocampal neurones in Alzheimer's disease. Neuropathol Appl Neurobiol 2002, 28:390–396
29. Muller-Hocker J: Cytochrome-c-oxidase deficient cardiomyocytes in the human heart—an age-related phenomenon. A histochemical ultracytochemical study. Am J Pathol 1989, 134:1167–1173
30. Tanaka M, Kovalenko SA, Gong JS, Borgeld HJ, Katsumata K, Hayakawa M, Yoneda M, Ozawa T: Accumulation of deletions and point mutations in mitochondrial genome in degenerative diseases. Ann NY Acad Sci 1996, 786:102–111
31. Cree LM, Samuels DC, de Sousa Lopes SC, Rajasimha HK, Wonnapinij P, Mann JR, Dahl HH, Chinnery PF: A reduction of mitochondrial DNA molecules during embryogenesis explains the rapid segregation of genotypes. Nat Genet 2008, 40:249–254
32. Adams I, Jones DG: Quantitative ultrastructural changes in rat cortical synapses during early-, mid- and late-adulthood. Brain Res 1982, 239:349–363
33. Chiti Z, Knutsen OM, Betmouni S, Greene JR: An integrated, temporal study of the behavioural, electrophysiological and neuropathological consequences of murine prion disease. Neurobiol Dis 2006, 22:363–373
34. Lustbader JW, Cirilli M, Lin C, Xu HW, Takuma K, Wang N, Caspersen C, Chen X, Pollak S, Chaney M, Trinchese F, Liu S, Gunn-Moore F, Lue LF, Walker DG, Kuppusamy P, Zewier ZL, Arancio O, Stern D, Yan SS, Wu H: ABAD directly links Abeta to mitochondrial toxicity in Alzheimer's disease. Science 2004, 304:448–452
35. Zhu D, Lai Y, Shelat PB, Hu C, Sun GY, Lee JC: Phospholipases A2 mediate amyloid-beta peptide-induced mitochondrial dysfunction. J Neurosci 2006, 26:11111–11119
36. Aiken JM, Williamson JL, Marsh RF: Evidence of mitochondrial involvement in scrapie infection. J Virol 1989, 63:1686–1694
37. Hachiya NS, Yamada M, Watanabe K, Jozuka A, Ohkubo T, Sano K, Takeuchi Y, Kozuka Y, Sakasegawa Y, Kaneko K: Mitochondrial localization of cellular prion protein (PrPC) invokes neuronal apoptosis in aged transgenic mice overexpressing PrPC. Neurosci Lett 2005, 374:98–103
38. Gray BC, Skipp P, O'Connor VM, Perry VH: Increased expression of glial fibrillary acidic protein fragments and mu-calpain activation within the hippocampus of prion-infected mice. Biochem Soc Trans 2006, 34:51–54
39. Almer G, Vukosavic S, Romero N, Przedborski S: Inducible nitric oxide synthase up-regulation in a transgenic mouse model of familial amyotrophic lateral sclerosis. J Neurochem 1999, 72:2415–2425
40. Stadelmann C, Ludwin S, Tabira T, Guseo A, Lucchinetti CF, Leel-Ossy L, Ordinario AT, Bruck W, Lassmann H: Tissue preconditioning may explain concentric lesions in Balo's type of multiple sclerosis. Brain 2005, 128:979–987
41. Bolanos JP, Almeida A, Fernandez E, Medina JM, Land JM, Clark JB, Heales SJ: Potential mechanisms for nitric oxide-mediated impairment of brain mitochondrial energy metabolism. Biochem Soc Trans 1997, 25:944–949
42. Cleeter MW, Cooper JM, Darley-Usmar VM, Moncada S, Schapira AH: Reversible inhibition of cytochrome c oxidase, the terminal enzyme of the mitochondrial respiratory chain, by nitric oxide. Implications for neurodegenerative diseases. FEBS Lett 1994, 345:50–54
43. Smith KJ, Lassmann H: The role of nitric oxide in multiple sclerosis. Lancet Neurol 2002, 1:232–241
44. Zhang J, Jin B, Li L, Block ER, Patel JM: Nitric oxide-induced persistent inhibition and nitrosylation of active site cysteine residues of mitochondrial cytochrome-c oxidase in lung endothelial cells. Am J Physiol Cell Physiol 2005, 288:C840–C849
45. Walsh DT, Betmouni S, Perry VH: Absence of detectable IL-1beta production in murine prion disease: a model of chronic neurodegeneration. J Neuropathol Exp Neurol 2001, 60:173–182
46. Cunningham C, Wilcockson DC, Campion S, Lunnon K, Perry VH: Central and systemic endotoxin challenges exacerbate the local inflammatory response and increase neuronal death during chronic neurodegeneration. J Neurosci 2005, 25:9275–9284
47. Picanco-Diniz CW, Boche D, Gomes-Leal W, Perry VH, Cunningham C: Neuropil and neuronal changes in hippocampal NADPH-diaphorase histochemistry in the ME7 model of murine prion disease. Neuropathol Appl Neurobiol 2004, 30:292–303
48. Sunico CR, Gonzalez-Forero D, Dominguez G, Garcia-Verdugo JM, Moreno-Lopez B: Nitric oxide induces pathological synapse loss by a protein kinase G-. Rho kinase-dependent mechanism preceded by myosin light chain phosphorylation. J Neurosci 2010, 30:973–984
49. Miele G, Jeffrey M, Turnbull D, Manson J, Clinton M: Ablation of cellular prion protein expression affects mitochondrial numbers and morphology. Biochem Biophys Res Commun 2002, 291:372–377
50. Lee DW, Sohn HO, Lim HB, Lee YG, Kim YS, Carp RI, Wisniewski HM: Alteration of free radical metabolism in the brain of mice infected with scrapie agent. Free Radic Res 1999, 30:499–507
51. Caron F, Jacq C, Rouviere-Yaniv J: Characterization of a histone-like protein extracted from yeast mitochondria. Proc Natl Acad Sci USA 1979, 76:4265–4269
52. Patel TB, Clark JB: Synthesis of N-acetyl-L-aspartate by rat brain mitochondria and its involvement in mitochondrial/cytosolic carbon transport. Biochem J 1979, 184:539–546
53. Broom KA, Anthony DC, Lowe JP, Griffin JL, Scott H, Blamire AM, Styles P, Perry VH, Sibson NR: MRI and MRS alterations in the preclinical phase of murine prion disease: association with neuropathological and behavioural changes. Neurobiol Dis 2007, 26:707–717
54. Paterson AW, Curtis JC, Macleod NK: Complex I specific increase in superoxide formation and respiration rate by PrP-null mouse brain mitochondria. J Neurochem 2008, 105:177–191
55. Lobao-Soares B, Bianchin MM, Linhares MN, Carqueja CL, Tasca CI, Souza M, Marques W, Jr., Brentani R, Martins VR, Sakamoto AC, Carlotti CG, Jr., Walz R: Normal brain mitochondrial respiration in adult mice lacking cellular prion protein. Neurosci Lett 2005, 375:203–206
56. Reeve AK, Krishnan KJ, Turnbull D: Mitochondrial DNA mutations in disease, aging, and neurodegeneration. Ann NY Acad Sci 2008, 1147:21–29
57. Davison AN, Dobbing J: Metabolic stability of body constituents. Nature 1961, 191:844–848